Article type : Original Article

Multifaceted Plant Reponses to Circumvent Phe Hyperaccumulation by Downregulation of Flux through the Shikimate Pathway and by Vacuolar Phe Sequestration

Joseph H. Lynch[1], Irina Orlova[2,†], Chengsong Zhao[3], Longyun Guo[1], Rohit Jaini[4], Hiroshi Maeda[2,‡], Tariq Akhtar[5,§], Junellie Cruz-Lebron[1], David Rhodes[2], John Morgan[1,4], Guillaume Pilot[3], Eran Pichersky[5] and Natalia Dudareva[1,2,6,*].

[1]Department of Biochemistry, Purdue University, West Lafayette, IN 47907, USA.

[2]Department of Horticulture and Landscape Architecture, Purdue University, West Lafayette, IN 47907, USA.

[3]Department of Plant Pathology, Physiology, and Weed Science, Virginia Tech, Blacksburg, VA 24061, USA

[4]School of Chemical Engineering, Purdue University, West Lafayette, IN 47907, USA.

[5]Department of Molecular, Cellular and Developmental Biology, University of Michigan, Ann Arbor, MI 48109, USA

[6]Purdue Center for Plant Biology, Purdue University, West Lafayette, IN 47907, USA.

[†]Present address: The Scotts Miracle-Gro Company, Marysville, OH 43041, USA

[‡]Present address: Department of Botany, University of Wisconsin – Madison, Madison, WI 53706-1313, USA

[§]Present address: Department of Molecular and Cellular Biology, University of Guelph, Guelph, Ontario, Canada N1G 2W1

[*]For correspondence (fax +1 765 494 0391; e-mail dudareva@purdue.edu)

Running title: Plant response to Phe hyperaccumulation

Key words: phenylalanine ammonia lyase, phenylalanine, phenylpropanoids, aromatic amino acids, shikimate pathway, *Petunia hybrida*, regulation

SUMMARY

Detrimental effects of hyperaccumulation of the aromatic amino acid phenylalanine (Phe) in animals, known as phenylketonuria, are mitigated by excretion of Phe derivatives; however, how plants endure Phe accumulating conditions in the absence of excretion system is currently unknown. To achieve Phe hyperaccumulation in a plant system, we simultaneous decreased in petunia flowers expression of all three Phe ammonia lyase (PAL) isoforms that catalyze the non-oxidative deamination of Phe to *trans*-cinnamic acid, the committed step for the major pathway of Phe metabolism. Total decrease in PAL activity by 81-94% led to an 18-fold expansion of the internal Phe pool. Phe accumulation had multifaceted intercompartmental effects on aromatic amino acid metabolism. It resulted in a decrease in the overall flux through the shikimate pathway, and a redirection of carbon flux toward the shikimate-derived aromatic amino acids tyrosine and tryptophan. Accumulation of Phe did not lead to an increase in flux toward phenylacetaldehyde, for which Phe is a direct precursor. Metabolic flux analysis revealed this to be due to the presence of a distinct metabolically inactive pool of Phe, likely localized in the vacuole. We have identified a vacuolar cationic amino acid transporter (*PhCAT2)* that contributes to sequestering excess of Phe in the vacuole. In vitro assays confirmed PhCAT2 can transport Phe, and decreased *PhCAT2* expression in *PAL*-RNAi transgenic plants resulted in 1.6-fold increase in phenylacetaldehyde emission. These results demonstrate mechanisms by which plants maintain intercompartmental aromatic amino acid homeostasis, and provide critical insight for future phenylpropanoid metabolic engineering strategies. (248)

INTRODUCTION

In mammals, hyperaccumulation of phenylalanine (Phe) leads to phenylketonuria (PKU), a degenerative neurological disorder that arises from a loss of phenylalanine hydroxylase activity (Williams et al. 2008). The buildup of Phe to toxic levels in PKU results in its conversion to phenylpyruvic acid and its derivatives, which are excreted with urine. Microbes prevent such accumulations through catabolism back to central carbon metabolism (Fuchs et al. 2011).

However, how plants tolerate high Phe levels in the absence of analogous excretion or catabolic systems remains unknown.

Under normal growth conditions, plants direct 20-30% of photosynthetically fixed carbon towards the shikimate pathway (Haslam 1993) and subsequently to biosynthesis of aromatic amino acids with the highest flux to Phe. In addition to being a building block for protein biosynthesis, Phe serves as a precursor for a multitude of phenolic compounds that have prominent, and often vital, roles in plant growth and development (*e.g.* lignin, suberin), reproduction (*e.g.* phenylpropanoids, benzenoids) and defense (*e.g.* salicylic acid, tannins, flavonoids). Constituting approximately 30-45% of plant organic matter (Razal et al. 1996), Phe-derived products are primarily synthesized in the cytosol but rely predominantly on Phe biosynthesis in and its export out of plastids (Widhalm et al. 2015; Maeda & Dudareva 2012).

In plants, Phe hyperaccumulation could be achieved by mutations in L-Phe ammonia lyase (PAL, EC 4.3.1.5) (Rohde et al., 2004), which catalyzes the first committed step, the nonoxidative deamination of Phe to *trans*-cinnamic acid, in the general phenylpropanoid pathway. PAL controls the carbon flux toward phenylpropanoid compounds and is often encoded by a small multigene family with four members in *Arabidopsis thaliana* (Raes et al. 2003) and *Nicotiana tabacum* (Reichert et al. 2009), and three members in *Petunia hybrida* (Colón et al. 2010). Expression of *PAL* genes is differentially and developmentally regulated, and is induced by biotic and abiotic stresses (Zhang & Liu 2015). Over the last decade, it has been shown that disruption of PAL activity leads to a decrease in downstream phenylpropanoid metabolism (Rohde et al. 2004; Huang, Gu, Lai, Fan, Shi, Y. Zhou, et al. 2010; Cass et al. 2015; Kim & Hwang 2014; Shi et al. 2010; Song & Wang 2011). However, the effect of accompanying Phe hyperaccumulation on Phe homeostasis is currently unknown.

Here we limited Phe utilization in *P. hybrida* cv Mitchell flowers by decreasing PAL activity via RNAi technology, and investigated its effects on upstream and downstream Phe metabolism. To avoid possible detrimental effects on plant vitality, a problem previously encountered upon systemic PAL perturbations in Arabidopsis (Huang, Gu, Lai, Fan, Shi, Y. Zhou, et al. 2010), metabolic manipulations were achieved specifically in the flowers by using a petal-specific promoter. Petunia flowers have high carbon flux through the phenylpropanoid network and emit high levels of exclusively Phe-derived volatiles (Boatright et al. 2004; Verdonk et al. 2003). They also contain phenylacetaldehyde synthase (PAAS) that catalyzes

phenylacetaldehyde formation directly from Phe and thus competes with PAL for Phe utilization (Kaminaga et al. 2006). The current results show that Phe hyperaccumulation affects carbon flux through the shikimate pathway and towards aromatic amino acids to maintain cytosolic Phe homeostasis. Similar flux redistribution occurs in Arabidopsis quadruple *pal* mutants, suggesting that these metabolic changes are not unique to petunia flowers. Moreover, excess Phe is not redirected towards phenylacetaldehyde formation, but rendered metabolically inactive by sequestration in the vacuole. Decreasing the expression of a newly identified *P. hybrida* vacuolar cationic amino acid transporter (PhCAT2) counteracts Phe sequestration in the vacuole of *PAL*-RNAi plants and makes it available to cytosolic enzymes.

RESULTS

Phe Hyperaccumulation Perturbs not Only Phenylpropanoid Metabolism but Also Aromatic Amino Acid Biosynthesis. Previously we showed that petunia flowers, which produce high levels of phenylpropanoid/benzenoid volatiles, express three PAL isoforms (Colón et al. 2010). While all three isoforms are highly similar in sequence (Figure S1), PAL1 displays the highest expression in petunia petals 2 days postanthesis, a stage of development with the highest levels of volatile phenylpropanoids, and PAL3 exhibits the lowest transcript level (Colón et al. 2010). To achieve Phe hyperaccumulation and to identify the role of PAL in regulation of Phe metabolism, we simultaneously decreased the expression of all three PAL genes in petunia by using a single RNAi construct (Figure S2a) under control of a petal specific promoter (Cseke et al. 1998). Out of multiple independent lines, two lines (11 and 26) showing the greatest reduction in *PAL* expression were selected for further metabolic profiling. Based on quantitative RT-PCR (qRT-PCR) with gene-specific primers, in line 11 expression of *PAL1, PAL2, and PAL3* were reduced by 98.5%, 92.0% and 93.5%, respectively, while their levels were decreased by 97.5%, 89.7% and 96.6%, respectively, in line 26 relative to control wild type flowers (Figure S2b), which were metabolically indistinguishable from empty vector control (Figure S3). *RNAi-PAL* suppression reduced PAL activity by 94% and 81% for lines 11 and 26, respectively, relative to controls (Figure 1). Flowers of the transgenic lines had a slight but statistically significant decrease in fresh weight relative to wild-type (Figure 1), otherwise the plants appeared morphologically unchanged.

Transgenic petals of both lines had 18-fold higher levels of Phe than wild type and drastically diminished emission of volatiles derived from *trans*-cinnamic acid (Figure 1). Emission of all phenylpropanoids/benzenoids was reduced in both transgenic lines relative to control, including a 85 to 99.5% reduction in emission benzaldehyde, benzylalcohol, benzylbenzoate, phenylethylbenzoate, methylbenzoate, eugenol and isoeugenol (Figure 1). Methylsalicylate emission was reduced by 47 to 65% in transgenic lines (Figure 1).

Reduction in PAL activity in both *PAL*-RNAi lines led to accumulation of Tyr and Trp, with levels increasing on average by 6.3 and 5.5-fold, respectively (Figure 1). Unexpectedly, the level of shikimic acid was significantly reduced in both transgenic lines relative to controls (by 74 to 88%), while phenylpyruvate level remained unchanged (Figure 1).

Reduction in PAL Activity Decreases Carbon Flux Through the Shikimate Pathway. To determine changes in flux through the shikimate pathway, wild type and line 11 petunia flowers were fed with uniformly ^{13}C-labeled ([U-$^{13}C_6$]) glucose and pool sizes and isotopic abundances of glucose, shikimate, and aromatic amino acids were analyzed at different time points over a 4-h period. The glucose labeling pattern was nearly identical in both control and transgenic petals (Figure 2). In both genotypes, glucose labeling always exceeded labeling of shikimate, consistent with a simple precursor-product relationship between sucrose and shikimate (Figure S4). Over this time course, the shikimate pool was significantly reduced in transgenic petals relative to the control, while there was little difference in its isotopic labeling (Figure S4). We have constructed a dynamic model of the aromatic amino acid biosynthetic network to reproduce the observations from ^{13}C-labeled glucose feeding for both wild type and *PAL*-RNAi flowers. Shikimate pathway flux estimated by the model was found to be 50.9% less in *PAL*-RNAi than wild type (Table 1). There is a corresponding decrease of 50.9% in flux towards Phe, while the fluxes toward Tyr and Trp are increased by 78.6% and 75.0%, respectively.

To assess whether the observed changes in flux through the shikimate pathway is the result of decreased expression of 3-deoxy-D-*arabino*-heptulosonate 7-phosphate synthase (DAHPS), which catalyzes the first committed step in the shikimate pathway (Bentley 1990; Herrmann & Weaver 1999), *DAHPS* transcript levels were analyzed in petals of two transgenic petunia lines and control plants. In addition, we examined the expression of genes down-stream of shikimate (e.g., 5-enolpyruvylshikimate 3-phosphate synthase, EPSPS) and those involved in Phe and Tyr

biosynthesis (chorismate mutase, CM1, and arogenate dehydratases, ADT1, ADT2 and ADT3), as well as the expression of the shikimate pathway transcriptional regulator, ODORANT1 (ODO1) (Verdonk et al. 2005). No statistically significant changes in *DAHPS*, *EPSPS*, *CM1* and *ODO1* transcript levels were observed in transgenic flowers relative to controls, although *ODO1* expression exhibited an apparent decreasing trend (Figure S5a). Transcript levels of the most highly expressed petunia ADT gene, *ADT1*, remained unaffected in flowers of transgenic lines, while *ADT2* and *ADT3* expression was increased only in line 11 (Figure S5b). However, total ADT activity was unaltered in either transgenic line (Figure S5b).

Perturbations in Aromatic Amino Acid Biosynthesis Following Phe Hyperaccumulation in Arabidopsis Stems Mirror Those of Petunia Petals. To determine whether the observed changes in the shikimate pathway flux and Phe biosynthesis as a result of Phe hyperaccumulation are unique to petunia petals, or if this might be a more general property of plants, we performed metabolic profiling of Arabidopsis stem from previously generated double *pal1pal2* and quadruple *pal1pal2pal3pal4* knockout mutants (Huang, Gu, Lai, Fan, Shi, Y. Zhou, et al. 2010). Similar to petunia petals, there is a high carbon flux toward phenylpropanoids in the Arabidopsis inflorescence stem, since it represents a major site of lignin biosynthesis. All four *PAL* genes are expressed in Arabidopsis stem with *AtPAL-3* displaying the lowest expression (Raes et al. 2003; Rohde et al. 2004). Metabolic profiling revealed that similar to *PAL*-RNAi petunia petals, in Arabidopsis quadruple *pal1pal2pal3pal4* knockout mutants the internal pools of three aromatic amino acids were drastically increased while shikimate level was decreased (Figure 3). The same trend was observed in double *pal1pal2* mutants and the degrees of changes were intermediate of wild type and the quadruple mutant (Figure 3).

Decreased *PAL* Expression Leads to the Accumulation of Phe that is Metabolically Inactive. Previously we have shown that petunia flowers produce phenylacetaldehyde by the action of a single cytosolic enzyme, PAAS, which catalyzes Phe decarboxylation-amine oxidation and competes with PAL for Phe utilization (Kaminaga et al. 2006). We also showed that feeding of petunia flowers with a range of concentrations of $^{2}H_5$-Phe led to a proportional increase in the internal pools of phenylacetaldehyde and its derivative 2-phenylethanol (Colón et al. 2010). Subsequently a kinetic model of the petunia phenylpropanoid/ benzenoid network was

developed to simulate the network responses to different concentrations of supplied Phe (Colón et al. 2010). Using this model we predicted that, although although kinetic constraints do not enable PAAS activity to prevent Phe accumulation, the observed increase in Phe levels in the *PAL*-RNAi lines should result in up to a 4-fold increase in phenylacetaldehyde emission (Figure S6a). However, no statistically significant changes were observed in phenylacetaldehyde and phenylethanol emission rates in transgenic lines relative to controls (Figure 1). This result was not due to a decrease in PAAS activity as it remained unchanged in transgenic plants (Figure S6b), suggesting that accumulated Phe is not accessible by PAAS in cytosol.

Moreover, feeding of petunia flowers from *PAL*-RNAi line 11 with uniformly labeled ^{13}C-glucose resulted in more rapid incorporation of label into the product, phenylacetaldehyde, than in its substrate, Phe (20.2% and 11.7% in 2 h, respectively) (Figure 4a). The observed labeling patterns further suggested that within the cell there is an inaccessible largely unlabeled Phe pool, which based on constructed dynamic flux model of the aromatic amino acid biosynthetic network was increased by 341% in the *PAL*-RNAi line 11 relative to wild type (Table 1). To determine the turnover of the metabolically inactive Phe pool, petunia petals were preloaded with ring-labeled $^{13}C_6$-Phe for 2 h (point 0 in Figure 4b) followed by a 6-h chase with unlabeled Phe, and intracellular Phe was analyzed for retention of the label. The $^{13}C_6$-Phe pool was depleted by 61% after 4 h of chase and remained unchanged thereafter. This lack of turnover further demonstrates that Phe is sequestered to a metabolically inactive pool.

Previous studies showed that Phe is present in vacuoles in Arabidopsis and barley plants (Krueger et al. 2011; Tohge et al. 2011). Thus, we hypothesized that the metabolically inactive Phe is located in the vacuole. To test this hypothesis, we analyzed Phe levels in vacuoles isolated from 1 day-old control and transgenic petunia flowers. Vacuole purity was verified by Western blot analysis with antibodies recognizing proteins specific to different subcellular compartments (Figure S7). Indeed, *PAL*-RNAi line 11 vacuoles exhibited a nearly 2-fold expansion in Phe content relative to wild type vacuoles (Figure 5a). In addition, we looked for petunia vacuolar transporters that might be involved in amino acid homeostasis. During our recent study to identify and characterize a plastidial Phe exporter (Widhalm et al. 2015), we also identified a contig, *Ph18042*, whose expression exhibited 2-fold increase in petunia petals on day 2 postanthesis relative to buds, the tissues with highest and lowest Phe levels, respectively. *Ph18042* was predicted to be localized to the vacuole and displays 71%/81% identity/similarity

to Arabidopsis vacuolar cationic amino acid transporter, AtCAT2 (Yang et al. 2014; Su et al. 2004). In the current investigation, the full-length sequence of *Ph18042* was fused to the N-terminus of the GFP reporter protein and transformed in *A. thaliana* expressing the tonoplast marker VAMP711-mCHERRY (Geldner et al. 2009) in order to experimentally determine its subcellular localization. Green fluorescence of the *Ph18042*-GFP in Arabidopsis leaf epidermis was co-localized with the red fluorescence of the tonoplast mCherry marker (Figure S8), suggesting that similar to Arabidopsis AtCAT2, Ph18042 (designated as PhCAT2) is localized in the tonoplast.

Neither PhCAT2 nor its more-studied homolog AtCAT2 have previously been directly tested for the ability to transport Phe. To test for ability of PhCAT2 to transport Phe, it was overexpressed in *Saccharomyces cerevisiae* mutants with gene deletions for the endogenous vacuolar amino acid transporters AVT1, AVT3, and AVT4. Vacuolar microsomes prepared from uncomplemented mutants were dramatically impaired in their ability to import Phe. However, PhCAT2 expression largely alleviated this impairment (Figure 5b). Ommitting ATP in the assay abolished the transport (Figure S9), similar to the situation previously shown for yeast transporters (Russnak et al. 2001), and for Phe uptake by isolated plant vacuoles (Homeyer & Schultz 1988). Together, these results confirm that PhCAT2 is a bonafide vacuolar Phe transporter.

To examine whether PhCAT2 contributes to sequestering excess Phe in the vacuole and thereby precluding its availability in the cytosol for phenylacetaldehyde production, *PhCAT2* expression was transiently decreased in wild-type and *PAL*-RNAi line 11 petunia flowers using *PhCAT2*-RNAi construct. A 70% reduction in *PhCAT2* expression in wild-type flowers (Figure 5c) resulted in no increase in phenylacetaldehyde emission, indicating little, if any, change in cytosolic Phe availability under normal conditions (Figure 5d). In contrast, a similar reduction in *PhCAT2* expression in a *PAL*-RNAi line 11 resulted in a 1.6-fold increase in phenylacetaldehyde emission, providing *in vivo* evidence that PhCAT2 transports the excess Phe from the cytosol into the vacuole.

Phe Hyperaccumulation Leads to Accumulation of New Phe-derived Compounds. GC-MS metabolic profiling of trimethylsilyl derived extracts revealed three peaks for which levels were increased 12-14 fold in the *PAL*-RNAi flowers relative to controls (Figure S10). ESI

fragmentation patterns were nearly identical for two of the three unknown peaks, and all three contain fragments consistent with the presence of the benzyl moiety (m/z 179 and 193). Furthermore, feeding with ring-labeled $^{2}H_5$-Phe resulted in a +5 mass shift in the m/z 179 and 193 ions, indicating that these compounds contain an unsubstituted aromatic ring derived from Phe. However, neither fragmentation patterns nor total masses matched with known compounds cataloged in the NIST databases (Figure S10). Additional attempts to identify these compounds by MALDI-TOF and LC-TOF were unsuccessful. The levels of each of these three compounds were estimated based on total ion current relative to internal standard assuming a similar response factor for Phe-derived compounds. Their levels ranged from 3 to 5% of the elevated Phe content in *PAL*-RNAi flowers.

DISCUSSION

In petunia flowers, as in lignifying plant tissues, a substantial portion of total carbon metabolic flux is directed through PAL, which catalyzes the entry step into the phenylpropanoid pathway. While in lignifying tissues PAL activity sustains lignin formation and production of other phenylpropanoids, in petunia flowers it enables the extensive production of phenylpropanoid/benzenoid volatiles, and in some cultivars anthocyanins, for pollinator attraction. Previously, it has been shown in Arabidopsis that decreased PAL activity results in a buildup of Phe (Huang, Gu, Lai, Fan, Shi, Y. Zhou, et al. 2010; Rohde et al. 2004) that is analogous to natural conditions in which aromatic amino acids accumulate in response to stress (Brouquisse et al. 1992; Kim et al. 2007; Saeed Saeedipour 2012). We show here that plants could activate mitigating mechanisms to prevent potential detrimental effects of such buildup. Our results indicate that decreased Phe utilization in the cytosol has multifaceted intercompartmental effects on aromatic amino acid metabolism that, as discussed below, occur in four ways: (*i*) by redirecting flux toward other aromatic amino acids, Trp and Tyr, which share common biosynthetic precursors in plastids; (*ii*) by decreasing production of Phe biosynthetic precursors (e.g. shikimate) in plastids; (*iii*) by sequestering Phe into a metabolically inactive pool in vacuole; and (*iv*) by converting Phe to unknown Phe-derived compounds.

Accumulation of Phe leads to decreased shikimate pathway flux and an increase in Tyr and Trp levels. The redirection of carbon flux towards Tyr and Trp as a result of feedback inhibition

by Phe of branch-point enzymes (i.e., chorismate mutase and arogenate dehydratase) within the plastidic aromatic amino acid network has been well documented (Widhalm et al. 2015; Goers & Jensen 1984; Maeda & Dudareva 2012; Eberhard et al. 1996). Therefore, it is likely that the redirection observed in the petunia *PAL*-RNAi plants is due to expansion of the plastidial Phe pool, suggesting that Phe accumulation in the cytosol led to a decrease in its export from plastids via the PhpCAT transporter. The observed lower shikimate levels in *PAL*-RNAi plants relative to controls (Figure 1) occurred without changes in transcript abundances of shikimate pathway biosynthetic genes (Figure S5), suggesting that posttranscriptional mechanisms regulate flux through the shikimate pathway. However, to date, little is known about how the carbon flow into the shikimate pathway is regulated in plants. While in microbes DAHP synthase, which catalyzes the entry step in the shikimate pathway, is subject to feedback regulation by aromatic amino acids, such a scenario has not yet been described in plants. Given that plant DAHP synthases belong to the type II class and contain aromatic amino acid-binding elements (Webby et al. 2010), it is possible that the correct conditions and/or combinations of aromatic amino acids under which plant DAHP synthase activity is affected have not yet been found. On the other hand, it is known that protein turnover of plant DAHP synthase and chorismate synthase can be regulated by the Clp protease system (Nishimura et al. 2013; Nishimura & van Wijk 2015). Recently a similar mechanism was shown to be involved in controlling accumulation of phenylpropanoids (Zhang et al. 2015) and flavonoids (Feder et al. 2015) via Kelch domain-containing F-box proteins. Thus, the precise mechanism(s) responsible for this observed decrease in flux through the shikimate pathway when PAL activity is decreased remain to be determined. It should be note that for nearly two decades it has been proposed that plants synthesize salicylic acid via two parallel pathways: Phe-dependent (via benzoate) and Phe-independent (via isochorismate) pathways (Huang, Gu, Lai, Fan, Shi, Y. Zhou, et al. 2010). A *PAL* mutant approach was used to distinguish the contribution of these two pathways to salicylic acid biosynthesis. However, our results show that such approach may lead to misleading conclusions, since in *PAL* mutants not only the flux through the Phe-dependent pathway is reduced, but also via the Phe-independent isochorismate pathway, for which shikimate is an immediate precursor.

Some accumulated Phe is sequestered in the vacuole. Reduction of PAL activity in the plant cell is similar to PKU in mammals caused by a loss of Phe hydroxylase activity and the resulting

inability to convert Phe to Tyr (Williams et al. 2008). In both cases the loss of a dominant pathway for Phe consumption leads to its hyperaccumulation. Animals eliminate excess of Phe by converting it predominantly to phenylpyruvate, followed by its excretion in the urine. In contrast, plants lack the secretory system, although they contain phenylpyruvate aminotransferase, PhPPY-AT, which catalyzes the reversible conversion of phenylpyruvate to Phe (Yoo et al. 2013). Phenylpyruvate levels in *PAL*-RNAi plants were unchanged relative to wild-type (Figure 1), indicating that accumulated Phe is likely unavailable for PPY-AT. Similarly, no significant differences were observed in the amount of Phe-derived metabolites, phenylacetadehyde and phenylethanol, emitted from the wild type and *PAL*-RNAi transgenic lines ($P>0.05$), despite the pronounced effect on cinnamic-acid derived compounds. Significantly, phenylacetaldehyde was labeled to a higher degree than its immediate substrate, Phe, after feeding with ^{13}C-glucose (Figure 4a), further suggesting the presence of a metabolically inactive Phe pool. Pulse chase experiments with $^{13}C_6$-Phe indicated a low turnover of this pool (Figure 4b), which is likely located in the vacuole (Figure 6). The presence of small but measurable Phe pool in the vacuole was previously shown in wild-type Arabidopsis plants by a non-aqueous fractionation (Krueger et al. 2011) and in barley by metabolomic analysis of isolated vacuoles (Tohge et al. 2011), and confirmed in petunia here (Figure 5a). Furthermore, we show that the vacuolar cationic amino acid transporter *PhCAT2* is capable of transporting Phe, and that decreasing *PhCAT2* expression in *PAL*-RNAi petunia flowers, achieved via RNAi strategy, led to an increase in the levels of the cytosolic Phe pool and subsequently in phenylacetaldehyde production (Figure 5c-d). Overall, the demonstration of this metabolically inactive pool of Phe in the vacuole provides insight into the fate of excess Phe under conditions in which its accumulation is stimulated. It also suggests a potential source of Phe for metabolic engineering strategies.

Some accumulated Phe is converted to unknown metabolites. We also noted the accumulation in petunia *PAL-RNAi* lines of three unknown compounds whose mass spectra and isotopic labeling indicate that they were derived from Phe. These compounds were present in wild-type petunia flowers at very low levels. It is not yet clear whether their accumulation is due to activation of a physiologically relevant Phe catabolic route, or merely induction of "silent metabolism" (Lewinsohn & Gijzen 2009) by the high Phe levels. However, both possibilities

must be considered in future metabolic engineering strategies which seek to increase production of Phe and valuable downstream metabolites.

EXPERIMENTAL PROCEDURES

Vector construction

RNAi mediated knockdown of all three PAL genes was achieved by targeting coding regions specific to PAL1 (nucleotides 923-1453, including an intron), PAL2 (nucleotides 81-440), and PAL3 (nucleotides 498-829) with a synthetic cDNA hairpin construct, generated as follows. The 1223 bp synthetic cDNA containing PAL isoforms specific regions described above was introduced into a modified pUC57 vector (pUC57-simple, Genscript, NJ) to create pUC57ConA. Using pUC57ConA as a template, a shorter fragment corresponding to nucleotides 1-1019 without intron was generated by PCR with primers RN1 and RN2 (see Supplementary Table S1). The amplicon was cloned between the AscI and BamHI sites of pUC57ConA in an antisense orientation, thus completing the hairpin construct targeting all three PAL genes. The resulting hairpin fragment was released from pUC57ConA by XhoI/BamHI digestion and ligated into the corresponding sites of the modified pRNA69 vector (Orlova et al. 2006) between the Clarkia breweri linalool synthase (LIS) petal-specific promoter and ocs terminator. The entire cassette was released by SacI/NotI digestion and ligated into the corresponding sites of the binary vector pART27.

For the PhCAT2-RNAi construct, DNA containing two spliced PhCAT2 cDNA fragments of the coding region corresponding to nucleotides 42-590 and 42-381, the latter in antisense orientation to create a hairpin structure, was synthesized (Genscript, NJ). 5′-EcoRI and 3′-BamHI sites were added for directional subcloning into pRNA69 containing LIS promoter. The resulting cassette containing the LIS promoter and the synthetic PhCAT2 hairpin fragment was released by SacI/SpeI digestion and subcloned into the corresponding sites of the binary vector pART27.

Plant material and transformation

Petunia (*Petunia hybrida* cv Mitchell, Ball Seed, http://www.ball-seed.com/) was used for the generation of transgenic plants. Plants were grown under a 16-h photoperiod in standard greenhouse conditions (Koeduka et al. 2008; Maeda et al. 2010). Transgenic plants were

obtained via Agrobacterium tumefaciens (strain EHA 105 carrying plasmid pART27-ConA) leaf disk transformation (Horsch et al. 1985). Plants, rooted on kanamycin selection, were screen by NPTII ELISA (Agdia Inc, Elkhart, IN, USA http://www.agdia.com) for neomycin phosphotransferase II and by PCR for the presence of the LIS promoter with the specific forward and reverse primers, LIS-F and LIS-R (Table S1). T0 and T1 transformants were self-pollinated and analyzed for segregation by germinating seeds on half-strength MS medium supplemented with kanamycin (200 mg/L). Untransformed petunia plants were used as a control in all described experiments. Transient transformation was carried out by floral infiltration as described previously (Yoo et al. 2013).

Arabidopsis were grown in growth chambers at 22°C and 120 µE m-2 s-1 light under a 12-h-light photoperiod. Arabidopsis pal mutants were generated previously (Huang, Gu, Lai, Fan, Shi, Y.-H. Zhou, et al. 2010) and were kindly provided to us by Dr. Z. Chen (Purdue University). Homozygous pal quadruple mutants were identified by PCR using PAL2 specific primers, pal 2-2-RP and pal 2-3-RP, and T-DNA-specific primers, pal 2-2-LB and pal 2-3-LB (Table S1).

RNA extraction, cDNA synthesis, and quantitative real time PCR

Total RNA was isolated from petal tissue using RNeasy Plant Mini Kit (Qiagene, Hilden, Germany). Each biological replicate contained a minimum of ten 2-d old corollas harvested at 8 PM and immediately frozen in liquid nitrogen. Total RNA was treated with DNase I using TURBO DNA-free kit (Ambion, MA), and 1 µg of DNA-free RNA was reverse transcribed using the High Capacity cDNA transcription kit (Applied Biosystems, CA). Gene-specific primers for each PAL gene (Table S1) were designed using PrimerExpress (Applied Biosystems, CA) and showed 90 to 100% efficiency at a final concentration of 300 nM. qRT-PCR was performed as described previously (Maeda et al. 2010). For relative quantification of PAL1, PAL2, and PAL3 transcript levels, UBQ10 was used as a reference gene (Maeda et al. 2010). Each data point represents an average three independent biological samples.

Enzyme assays

PAL, PAAS and ADT activities were measured in crude protein extracts prepared from petunia petals of control and transgenic plants harvested at 8 PM, day 2 after anthesis as described previously (Maeda et al. 2010). ADT activity was analyzed in the petunia petal plastidial fraction

isolated as described before (Yoo et al. 2013). Plastids were suspended in 500 µL of ADT assay buffer (250mM sodium phosphate buffer, pH 8.2, 1mM EDTA), soluble crude protein extract was desalted into ADT assay buffer with Sephadex G50 to remove metabolites, and assayed for ADT as previously described (Maeda et al. 2010).

Analysis of volatiles, organic acids, and aromatic amino acids

Volatile compounds were collected from control and PAL-RNAi petunia flowers for 12 hours starting at 8 pm 2 days post-anthesis using the closed-loop stripping method (Orlova et al. 2006) and analyzed by GC-MS (Agilent, CA) as described previously (Maeda et al. 2010). For organic and aromatic amino acid analysis, approximately 0.5 g of frozen tissue as extracted overnight at 4°C with 10 ml of 100% methanol. A100 µl aliquot of methanol extract was analyzed at the Metabolomic Center of the University of Illinois at Urbana-Champaign for aromatic amino acids, benzoic acid, phenylpyruvic acid and shikimic acid. Chromotographic separation was achieved by HPLC using a Phenyl column (100 x 4.6 mm, 3µm) with a 6-min linear gradient of 1-95% acetonitrile in 25 mM ammonium acetate at a 0.4 ml/min flow rate. Quantification was performed using calibration curves generated from individual authentic standards.

Stable isotope labeling experiments

Corollas excised from flowers 2 days post-anthesis were placed on filter paper moistened with 2 ml of the requisite labeled compound, as described in results. Emitted and internal pools of volatiles were collected as described above. Phe was extracted and analyzed by LC-MS as described previously (Yoo et al. 2013). Glucose and shikimate were analyzed as described previously (Maeda et al. 2010), except that shikimate was extracted from tissue in 70% (v/v) methanol. The fractional labeling percentage of each compound was determined by comparison of the intensity of the shifted molecular ions and corrected for the natural isotope abundance.

Isolation of Petunia Vacuoles

Protoplasts were isolated from petal limbs of petunia flowers 1-day post-anthesis as described previously (Faraco et al. 2011). Protoplasts were lysed and vacuoles were purified as described previously (Robert et al. 2007), except protoplast lysis buffer contained 250 mM mannitol. Western blot analysis was performed using petal crude extracts and lyophilized vacuoles

resuspended in 1 x Laemmli buffer. Immunodetection was perfomed using rabbit primary polyclonal antibodies raised against organelle-specific markers (Agrisera, Sweden). Antigen bands were visualized using Immun-Blot Goat Anti-Rabbit IgG (H + L)-AP Assay Kit (Bio-Rad) according to the manufacturer's protocol.

Yeast Transport Assays

AVT1, *AVT3*, and *AVT4* genes, shown to be involved in amino acid transport at the vacule (Sekito et al. 2008) were deleted from *Saccharomyces cerevisiae* strain BY4741 (*MAT*a *his3Δ1 leu2Δ0 met15Δ0 ura3Δ0*) by recombination with amplicons of the *loxP-KanMX-loxP* cassette (Güldener et al. 1996), *lox2272–natNT2–lox2272*, and *loxLE–hphNT1–loxRE* (Carter & Delneri 2010), respectively, generated by PCR with primers in Table S1. Gene deletions were confirmed by PCR using primers in Table S1. Yeast vacuole purification and Phe transport assays were performed according to (Russnak et al. 2001), using PhCAT2 cloned into the gateway compatible yeast expression vector pDR196 (Loqué et al. 2007).

Metabolic flux modeling

Aromatic amino acid biosynthesis was simplified as three parallel macro-reactions, each converts common precursor glucose into Phe, Tyr or Trp. Equations of three reactions focused on carbon mass balance were:

$1.67\ Glucose \xrightarrow{v_1} Phe + CO_2$

$1.67\ Glucose \xrightarrow{v_2} Tyr + CO_2$

$2\ Glucose \xrightarrow{v_3} Trp + CO_2$

Aromatic amino acids were assumed to be the major sinks for the shikimate pathway, and therefore its flux during the feeding studies was estimated from the sum of the fluxes through those three reactions. All fluxes were assumed to be constant within four hour period of feeding time and metabolite concentration dynamics in the pathway can be captured by linear functions, which matched with corresponding time-course measurements. An empirical function was applied to simulate glucose labeling percentage dynamics and v1 was constrained by known Phe-derived volatile emission rates. Inclusion of a metabolically inactive pool parameter for Phe improved fit with experimental observations. In total, 11 unknown parameters were estimated for each case. Detailed involvements of these parameters into the model are listed below:

$$C_{Phe_{interactive,t}} = \theta_1 + \frac{\theta_2 - \theta_1}{4} * t$$

$$C_{Tyr_t} = \theta_3 + \frac{\theta_4 - \theta_3}{4} * t$$

$$C_{Trp_t} = \theta_5 + \frac{\theta_6 - \theta_5}{4} * t$$

$$f_{Glucose_t} = \theta_7 * (1 - e^{-\theta_8 * t})$$

$$v_1 = v_{emission} + \frac{\theta_2 - \theta_1}{4}$$

$$v_2 = \theta_9$$

$$v_3 = \theta_{10}$$

$$C_{Phe_{uninteractive}} = \theta_{11}$$

For each aromatic amino acid, labeling percentage dynamics were numerically integrated with following balance equations (Widhalm et al. 2015) by ode15 solver in Matlab R2013a (The MathWorks, Inc., Natick, MA):

$$\frac{df_{Phe_{interactive,t}}}{dt} = \frac{\left(f_{Glucose_t} - f_{Phe_{interactive,t}}\right) * v_1}{C_{Phe_{interactive,t}}}$$

$$\frac{df_{Tyr_t}}{dt} = \frac{\left(f_{Glucose_t} - f_{Tyr_t}\right) * v_2}{C_{Tyr_t}}$$

$$\frac{df_{Trp_t}}{dt} = \frac{\left(f_{Glucose_t} - f_{Trp_t}\right) * v_3}{C_{Trp_t}}$$

To enable direct comparison of the model's outputs with experimental measurements, the metabolically inactive Phe pool was integrated into the final outputs as follows:

$$C_{Phe_t} = C_{Phe_{interactive,t}} + C_{Phe_{uninteractive,t}}$$

$$f_{Phe_t} = f_{Phe_{interactive,t}} * \frac{C_{Phe_{interactive,t}}}{C_{Phe_t}}$$

The objective function was defined as the differences between model predicted profiles and experimentally measured profiles, weighed by the measurement variances. Parameters were estimated by minimizing the objective function through lsqnonlin function in Matlab R2013a with multi-run approach. The mathematical representation of the optimization process is shown below:

$$\theta = arg\min_{\theta} \sum \frac{(Profile_{simulated} - Profile_{measured})^2}{s^2_{Profile_{measured}}}$$

Parameter uncertainty analysis was also performed as described in (Press 2007). Briefly, 5,000 synthetic datasets were generated based on average and variance for each measurement by assuming a Gaussian distribution. For each dataset, same optimization process was performed to obtain parameter values, and parameter uncertainty as well as model predicted profile variance was estimated based on the variance of 5,000 parameter sets.

Subcellular localization of PhCAT2

The full length coding sequence of PhCAT2 was amplified using forward and reverse primers, PhCAT2-F and PhCAT2_NSR, respectively (Supplementary Table S1), both of which include primer extensions for SfiI recognition sites. The resulting fragment was subcloned into SfiI sites of pENTR223, sequence verified and transferred into pK7FWG2 via GatewayTM technology, resulting in an in-frame fusion with the N-terminal end of GFP. The PhCAT2-GFP construct was stably transformed via Agrobacterium-mediated floral dip into A. thaliana expressing the tonoplast marker VAMP711-mCHERRY (Geldner et al. 2009). T1 plants surviving kanamycin selection were imaged. Images were acquired using a Zeiss LSM710 laser spectral scanning confocal microscope with a C-Apochromat 40 × /1.20 W objective (Zeiss, NY). GFP was excited with an argon laser at wavelength 488 nm and emissions were collected over a 493–598-nm bandpass. mCherry was excited at wavelength 561 nm and emissions were collected over 600-680 nm bandpass. Chlorophyll fluorescence was excited by a HeNe laser at wavelength 633 nm and emissions were collected over a 647–721-nm bandpass.

Accession number

The GenBank/EMBL accession numbers for the sequences mentioned in this article are as follows: KX817349

ACKNOWLEDGMENTS

This work was supported by a grant from the National Science Foundation MCB-1519083 to ND. We thank Dr. Zhixiang Chen for providing seeds of Arabidopsis *pal* mutants, and Dr.

Francesca Quattrocchio and Shuanjiang Li for advising on the isolation of protoplasts. The authors declare no conflict of interest.

SHORT SUPPORTING INFORMATION LEGENDS

Figure S1. Protein sequence alignment for the three *Petunia hydrida, cv Mitchell* PAL isoforms.

Figure S2. Generation of petunia *PAL* RNAi lines.

Figure S3. Metabolic analysis of empty vector control petunia flowers.

Figure S4. Isotopic abundances and pool sizes of shikimate in control and *PAL*-RNAi petunia flowers during feeding with [U-$^{13}C_6$]-glucose.

Figure S5. Expression levels of genes encoding enzymes involved in aromatic amino acid biosynthesis and ODO1 transcription factor in control and *PAL*-RNAi petunia flowers.

Figure S6. Model simulated and experimentally determined phenylacetaldehyde emission in transgenic *PAL*-RNAi flowers.

Figure S7. Representative western blot analysis of purity of isolated vacuoles.

Figure S8. Subcellular localization of PhCAT2.

Figure S9. ATP dependence of Phe transport by yeast vacuolar microsomes.

Figure S10. Representative GC-MS chromatograms of trimethylsilyl (TMS)-derived extracts obtained from control and *PAL*-RNAi petunia flowers.

Table S1. Sequences of primers used for cloning, genotyping, and qRT-PCR.

REFERENCES

Bentley, R., 1990. The shikimate pathway - metabolic tree with many branches. *Critical Reviews in Biocheistry and Molecular Biology*, 25(5), pp.307–383.

Boatright, J. et al., 2004. Understanding in vivo benzenoid metabolism in petunia petal tissue. *Plant Physiology*, 135(4), pp.1193–2011.

Brouquisse, R. et al., 1992. Asparagine metabolism and nitrogen distribution during protein degradation in sugar-starved maize root-tip. *Planta*, 188(3), pp.384–395.

Carter, Z. & Delneri, D., 2010. New generation of loxP-muta ted deletion cassettes for the genetic manipulation of yeast natural isolates. *Yeast*, 27(9), pp.765–775.

Cass, C.L. et al., 2015. Effects of phenylalanine ammonia lyase (PAL) knockdown on cell wall composition, biomass digestibility, and biotic and abiotic stress responses in Brachypodium.

Journal of Experimental Botany, 66(14), pp.4317–4335.

Colón, A.M. et al., 2010. A kinetic model describes metabolic response to perturbations and distribution of flux control in the benzenoid network of Petunia hybrida. *Plant Journal*, 62(1), pp.64–76.

Cseke, L., Dudareva, N. & Pichersky, E., 1998. Structure and evolution of linalool synthase. *Molecular biology and evolution*, 15(11), pp.1491–1498.

Eberhard, J. et al., 1996. Cytosolic and plastidic chorismate mutase isozymes from Arabidopsis thaliana: molecular characerization and enzymatic properties. *The Plant Journal*, 10(5), pp.815–821.

Faraco, M. et al., 2011. One protoplast is not the other! *Plant Physiology*, 156(2), pp.474–478.

Feder, A. et al., 2015. A Kelch domain-containing F-box coding gene negatively regulates flavonoid accumulation in muskmelon. *Plant Physiology*, 169(3), pp.1714–1726.

Fuchs, G., Boll, M. & Heider, J., 2011. Microbial degradation of aromatic compounds — from one strategy to four. *Nature Reviews Microbiology*, 9(11), pp.803–816. Available at: http://dx.doi.org/10.1038/nrmicro2652.

Geldner, N. et al., 2009. Rapid, combinatorial analysis of membrane compartments in intact plants with a multicolor marker set. *The Plant Journal*, 59, pp.169–178.

Goers, S.K. & Jensen, R.A., 1984. The differential allosteric regulation of two chorismate-mutase isoenzymes of Nicotiana silvestris. *Planta*, 162, pp.117–124.

Güldener, U. et al., 1996. A new efficient gene disruption cassette for repeated use in budding yeast. *Nucleic acids research*, 24(13), pp.2519–2524.

Haslam, E., 1993. *Shikimic Acid: Metabolism and Metabolites*, John Wiley & Sons Inc.

Herrmann, K.M. & Weaver, L.M., 1999. The shikimate pathway. *Annual Review of Plant Physiology and Plant Molecular Biology*, 50, pp.473–503.

Homeyer, U. & Schultz, G., 1988. Transport of phenylalanine into vacuoles isolated from barley mesophyll protoplasts. *Planta*, 176(3), pp.378–382.

Horsch, R.B. et al., 1985. A simple and general method for transferring genes into plants. *Science*, 227(4691), pp.1229–1231.

Huang, J., Gu, M., Lai, Z., Fan, B., Shi, K., Zhou, Y., et al., 2010. Functional analysis of the Arabidopsis PAL gene family in plant growth, development, and response to environmental stress. *Plant Physiology*, 153, pp.1526–1538.

Huang, J., Gu, M., Lai, Z., Fan, B., Shi, K., Zhou, Y.-H., et al., 2010. Functional analysis of the Arabidopsis PAL gene family in plant growth, development, and response to environmental stress. *Plant physiology*, 153(4), pp.1526–1538.

Kaminaga, Y. et al., 2006. Plant phenylacetaldehyde synthase is a bifunctional homotetrameric enzyme that catalyzes phenylalanine decarboxylation and oxidation. *Journal of Biological Chemistry*, 281(33), pp.23357–23366.

Kim, D.S. & Hwang, B.K., 2014. An important role of the pepper phenylalanine ammonia-lyase gene (PAL1) in salicylic acid-dependent signalling of the defence response to microbial pathogens. *Journal of Experimental Botany*, 65(9), pp.2295–2306.

Kim, S.W. et al., 2007. Metabolic discrimination of sucrose starvation from Arabidopsis cell suspension by 1H NMR based metabolomics. *Biotechnology and Bioprocess Engineering*, 12(6), pp.653–661.

Koeduka, T. et al., 2008. The multiple phenylpropene synthases in both Clarkia breweri and Petunia hybrida represent two distinct protein lineages. *The Plant Journal*, 54, pp.362–374.

Krueger, S. et al., 2011. A topological map of the compartmentalized Arabidopsis thaliana leaf metabolome. *PLoS ONE*, 6(3), p.e17806.

Lewinsohn, E. & Gijzen, M., 2009. Phytochemical diversity: The sounds of silent metabolism. *Plant Science*, 176(2), pp.161–169.

Loqué, D. et al., 2007. A cytosolic trans-activation domain essential for ammonium uptake. *Nature*, 446(7132), pp.195–198.

Maeda, H. et al., 2010. RNAi Suppression of Arogenate Dehydratase1 Reveals That Phenylalanine Is Synthesized Predominantly via the Arogenate Pathway in Petunia Petals. *The Plant Cell*, 22(3), pp.832–849.

Maeda, H. & Dudareva, N., 2012. The shikimate pathway and aromatic amino acid biosynthesis in plants. *Annual Review of Plant Biology*, 63, pp.73–105.

Nishimura, K. et al., 2013. ClpS1 is a conserved substrate selector for the chloroplast Clp protease system in Arabidopsis. *The Plant cell*, 25(6), pp.2276–301. Available at: http://www.ncbi.nlm.nih.gov/pubmed/23898032.

Nishimura, K. & van Wijk, K.J., 2015. Organization, function and substrates of the essential Clp protease system in plastids. *Biochimica et biophysica acta*, 1847(9), pp.915–930. Available at: http://dx.doi.org/10.1016/j.bbabio.2014.11.012.

Orlova, I. et al., 2006. Reduction of benzenoid synthesis in petunia flowers reveals multiple pathways to benzoic acid and enhancement in auxin transport. *The Plant cell*, 18, pp.3458–3475.

Press, W.H., 2007. *Numerical Recipes: The Art of Scientific Computing* 3rd ed., Cambridge University Press.

Raes, J. et al., 2003. Genome-wide characterization of the lignification toolbox in Arabidopsis. *Plant Physiology*, 133(3), pp.1051–1071. Available at: http://www.scopus.com/inward/record.url?eid=2-s2.0-0142035247&partnerID=40&md5=e4e081e08156acbc208e15a29bc16846%5Cnhttp://www.plantphysiology.org/content/133/3/1051.full%5Cnhttp://www.plantphysiology.org/content/133/3/1051.short.

Razal, R.A. et al., 1996. Nitrogen recycling in phenylpropanoid metabolism. *Phytochemistry*, 41(1), pp.31–35.

Reichert, A.I., He, X. & Dixon, R.A., 2009. Phenylalanine ammonia-lyase (PAL) from tobacco (Nicotiana tabacum): characterization of the four tobacco PAL genes and active heterotetrameric enzymes. *Biochemical Journal*, 242(2), pp.233–242.

Robert, S. et al., 2007. Isolation of intact vacuoles from Arabidopsis rosette leaf–derived protoplasts. *Nature Protocols*, 2(2), pp.259–262.

Rohde, A. et al., 2004. Molecular phenotyping of the pal1 and pal2 mutants of Arabidopsis thaliana reveals far-reaching consequences on phenylpropanoid, amino acid, and carbohydrate metabolism. *The Plant cell*, 16(10), pp.2749–2771.

Russnak, R., Konczal, D. & McIntire, S.L., 2001. A family of yeast proteins mediating bidirectional vacuolar amino acid transport. *Journal of Biological Chemistry*, 276(26), pp.23849–23857.

Saeed Saeedipour, 2012. Stress-induced changes in the free amino acid composition of two wheat cultivars with difference in drought resistance. *African Journal of Biotechnology*, 11(40), pp.9559–9565.

Sekito, T. et al., 2008. Novel families of vacuolar amino acid transporters. *IUBMB life*, 60(8), pp.519–525.

Shi, R. et al., 2010. Specific down-regulation of PAL genes by artificial microRNAs in populus trichocarpa. *Planta*, 232(6), pp.1281–1288.

Song, J. & Wang, Z., 2011. RNAi-mediated suppression of the phenylalanine ammonia-lyase gene in Salvia miltiorrhiza causes abnormal phenotypes and a reduction in rosmarinic acid biosynthesis. *Journal of Plant Research*, 124(1), pp.183–192.

Su, Y., Frommer, W.B. & Ludewig, U., 2004. Molecular and functional characterization of a family of amino acid transporters from Arabidopsis. *Plant Physiology*, 136(2), pp.3104–3113.

Tohge, T. et al., 2011. Toward the storage metabolome: profiling the barley vacuole. *Plant Physiology*, 157(3), pp.1469–1482.

Verdonk, J.C. et al., 2005. ODORANT1 regulates fragrance biosynthesis in petunia flowers. *The Plant cell*, 17(5), pp.1612–1624.

Verdonk, J.C. et al., 2003. Regulation of floral scent production in petunia revealed by targeted metabolomics. *Phytochemistry*, 62, pp.997–1008.

Webby, C.J. et al., 2010. Synergistic allostery, a sophisticated regulatory network for the control of aromatic amino acid biosynthesis in Mycobacterium tuberculosis. *Journal of Biological Chemistry*, 285(40), pp.30567–30576.

Widhalm, J.R. et al., 2015. Identification of a plastidial phenylalanine exporter that influences flux distribution through the phenylalanine biosynthetic network for bioenergy. *Nature Communications*, 6.

Williams, R.A., Mamotte, C.D.S. & Burnett, J.R., 2008. Phenylketonuria: an inborn error of phenylalanine metabolism. *The Clinical biochemist. Reviews / Australian Association of Clinical Biochemists*, 29(1), pp.31–41.

Yang, H. et al., 2014. Characterization of the putative amino acid transporter genes AtCAT2, 3 & 4: The tonoplast localized AtCAT2 regulates soluble leaf amino acids. *Journal of Plant Physiology*, 171(8), pp.594–601. Available at: http://dx.doi.org/10.1016/j.jplph.2013.11.012.

Yoo, H. et al., 2013. An alternative pathway contributes to phenylalanine biosynthesis in plants via a cytosolic tyrosine:phenylpyruvate aminotransferase. *Nature Communications*, 4. Available at: http://dx.doi.org/10.1038/ncomms3833.

Zhang, X. et al., 2015. Down-regulation of Kelch domain-containing F-box protein in Arabidopsis enhances the production of (poly)phenols and tolerance to ultraviolet radiation. *Plant Phy*, 167(2), pp.337–350.

Zhang, X. & Liu, C., 2015. Multifaceted regulations of gateway enzyme phenylalanine ammonia-lyase in the biosynthesis of phenylpropanoids. *Molecular Plant*, 8(1), pp.17–27. Available at: http://dx.doi.org/10.1016/j.molp.2014.11.001.

	Biosynthetic Fluxes (nmol/gFW/h)				Inactive Phe (nmol/gFW)
	Phe	Tyr	Trp	Shik	
Wild type	456.6±91.4	0.14±0.02	0.04±0.01	456.8±91.4	188.5±26.8
PAL-RNAi	224.2±37.2	0.25±0.05	0.07±0.03	224.5±37.2	830.9±71.7
Relative Change	-50.9%	+78.6%	+75.0%	-50.9%	+340.8%

Table 1. Model-predicted metabolic fluxes within the aromatic amino acid biosynthetic network. All parameter means and variances were obtained based on the values estimated from 5,000 synthetic datasets fit to experimentally determined label incorporation from exogenously supplied [U-$^{13}C_6$]-glucose over 4 hours, as described in supporting methods.

FIGURE LEGENDS

Figure 1. Effect of *PAL*-RNAi Suppression on flower morphology and aromatic amino acid and phenylpropanoid/benzenoid metabolism. Emitted volatiles (orange background) were collected from 20:00 to 08:00 and internal pools of organic (blue background) and aromatic amino acids (purple background) were extracted at 20:00 from control (black bars) and transgenic petunia *PAL*- RNAi lines 11 (gray bars) and 26 (white bars) flowers 2 days postanthesis. Results are presented as nmol/gFW/hr for emitted volatiles and nmol/gFW for internal pools. Data are means ± SE of a minimum of three biological replicates. Inset: Representative flowers of wild-type and *PAL*-RNAi lines 11 and 26 show a discernable decrease

in flower size in RNAi lines relative to WT (Bar = 1 cm). PAL activity and corolla fresh weights are given as the average ± SE. * P<.05, ** P<.01, *** P<0.001.

Figure 2. Dynamic model simulation and experimentally obtained pool sizes and labeling patterns for aromatic amino acids and glucose in wild type and *PAL*-RNAi petunia flowers. Isotopic abundances and pool sizes were analyzed over a 4-h time period (starting at 18:00) of [U-$^{13}C_6$]-glucose feeding to flowers of control (blue lines and symbols) and transgenic *PAL*-RNAi line 11 (red lines and symbols) plants. Lines represent simulation results, with shaded area reflecting 95% confidence area for model's outputs. Data points are the average of 3 biological replicates, error bars represent standard deviation.

Figure 3. Levels of aromatic amino acids and shikimate in *pal1pal2* double and *pal1pal2pal3pal4* quadruple Arabidopsis mutants. Black bar, wild type control; grey bar, *pal1pal2* double mutants; white bar, *pal1pal2pal3pal4* quadruple mutants. Data are means ± SE (n ≥ 4 biological replicates). * P<0.05, ** P<0.01, Shik, shikimate.

Figure 4. Isotopic labeling of Phe and phenylacetaldehyde from [^{13}C]-glucose and pulse/chase feeding of [^{13}C]-Phe/[^{12}C]-Phe to *PAL*-RNAi petunia flowers. (a) Labeling kinetics of Phe and phenylacetaldehyde over a 6-h time period, beginning at 18:00, of feeding *PAL*-RNAi line 11 flowers with [U-$^{13}C_6$]-glucose. Label incorportation into Phe is shown with black diamonds and into phenylacetaldehyde with white circles. (b) Results of pulse-chase experiments. Flowers of *PAL*-RNAi line 11 were pre-fed for 2 h with 75 mM [$^{13}C_6$]-Phe before being transferred to 75 mM unlabeled Phe at time=0 (18:00). Internal pools of labeled (black triangles) and unlabeled (black squares) Phe, as well as its isotopic abundance (white diamonds) were analyzed over 6-h period. All data are means ± SE (n=3 biological replicates). * P<0.05 as determined by unpaired two-tailed Student's t-tests between phenylacetaldehyde and Phe labeling.

Figure 5. Phe accumulates in vacuoles, and downregulation of vacuolar Phe transporter *PhCAT2* increases phenylacetaldehyde emission in petunia flowers. (a) Phe content of vacuoles purified from protoplasts that were isolated from wild type (WT) and and PAL-RNAi

line 11 flower petals on 1-day post-anthesis. (b) Phe transport assays in vacuole microsomes from wild type BY4741 yeast (squares), the corresponding avt1/3/4 triple mutant containing the empty vector (circles) and the avt1/3/4 mutant expressing PhCAT2 (triangles), in presence of ATP. Significance indicated relative to the avy1/3/4 triple mutant. (c) *PhCAT2* expression in wild type and *PAL*-RNAi line 11 flowers infiltrated with the empty vector (black bars) and the *PhCAT2* RNAi construct (grey bars). (d) Phenylacetaldehyde emission from flowers shown in (b) over the period from 16:00 to 20:00. Absolute value of empty vector control emission is 2.9 and 3.2 nmol h-1 g FW for wild type and *PAL*-RNAi line 11, respectively. For all panels, data are means ± SE (n≥3 biological replicates). * $P<0.05$, ** $P<0.011$, *** $P<0.001$ as determined by unpaired two-tailed Student's t-tests.

Figure 6: Proposed model of subcellular inter-compartmental Phe fluxes in petunia flowers.

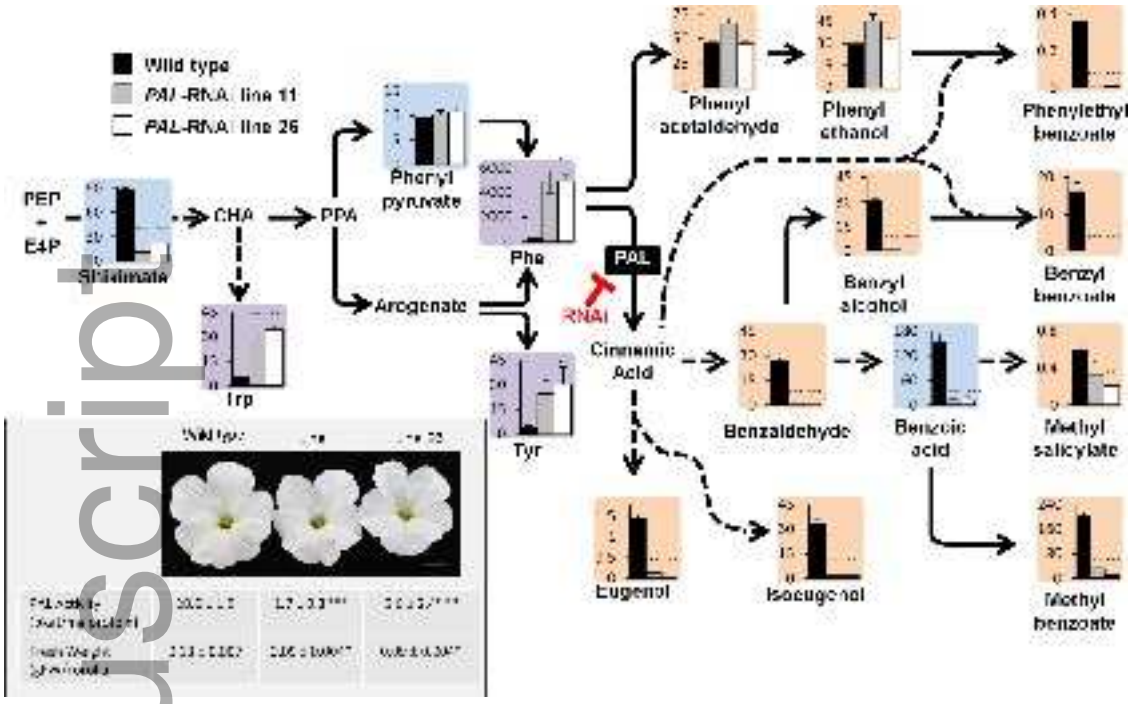

tpj_13730_f1.tif

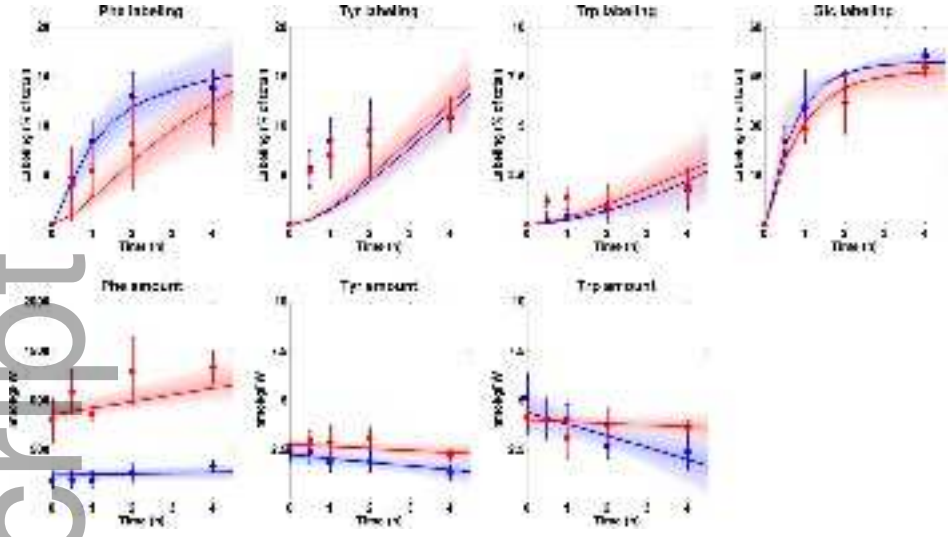

tpj_13730_f2.tif

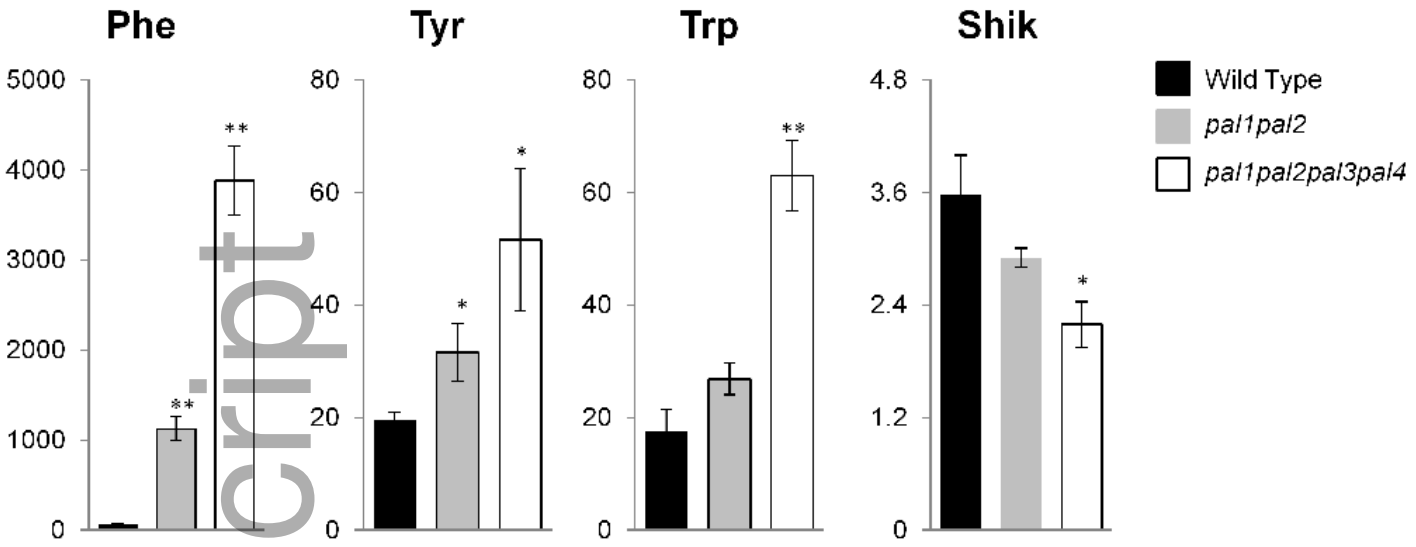

tpj_13730_f3.tif

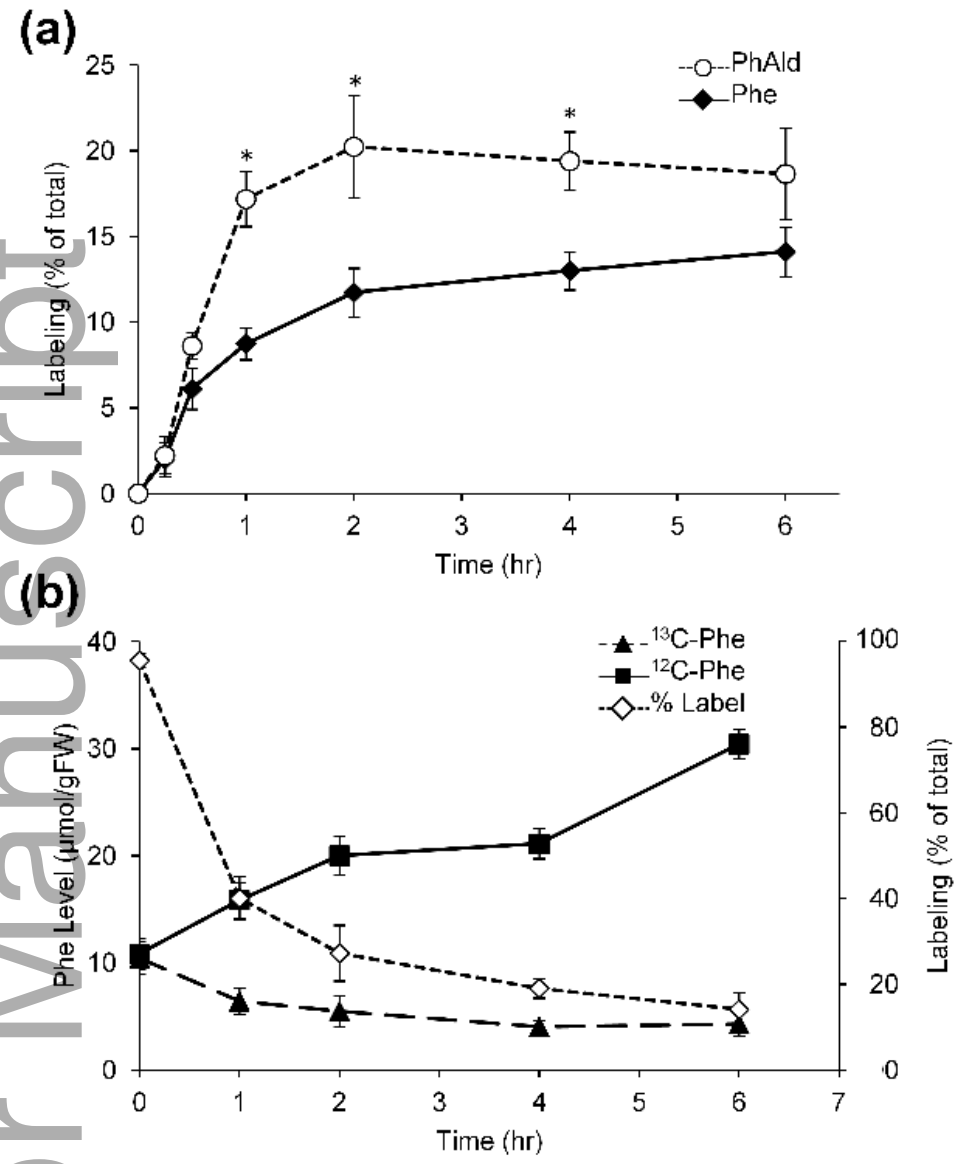

tpj_13730_f4.tif

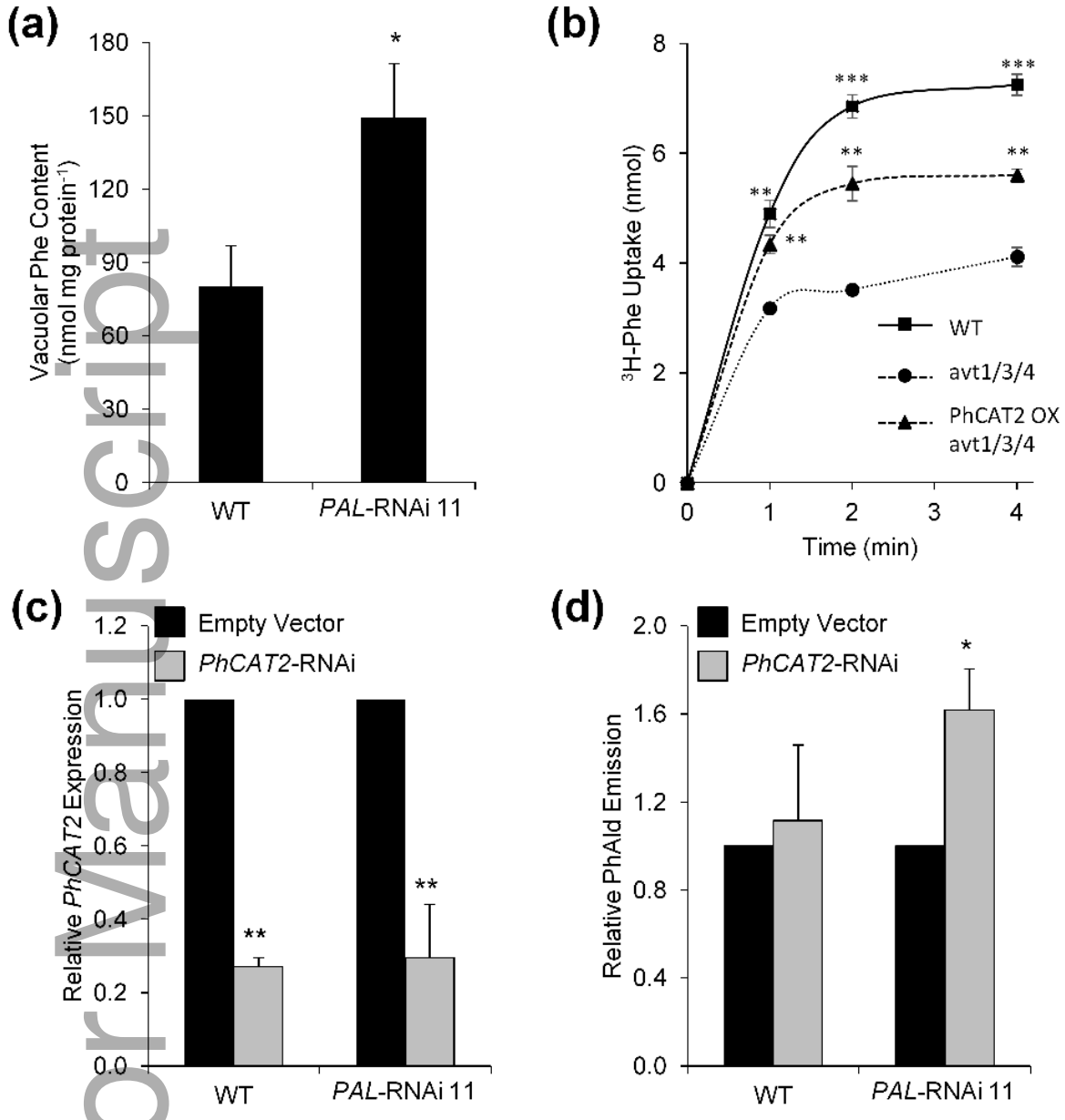

tpj_13730_f5.tif

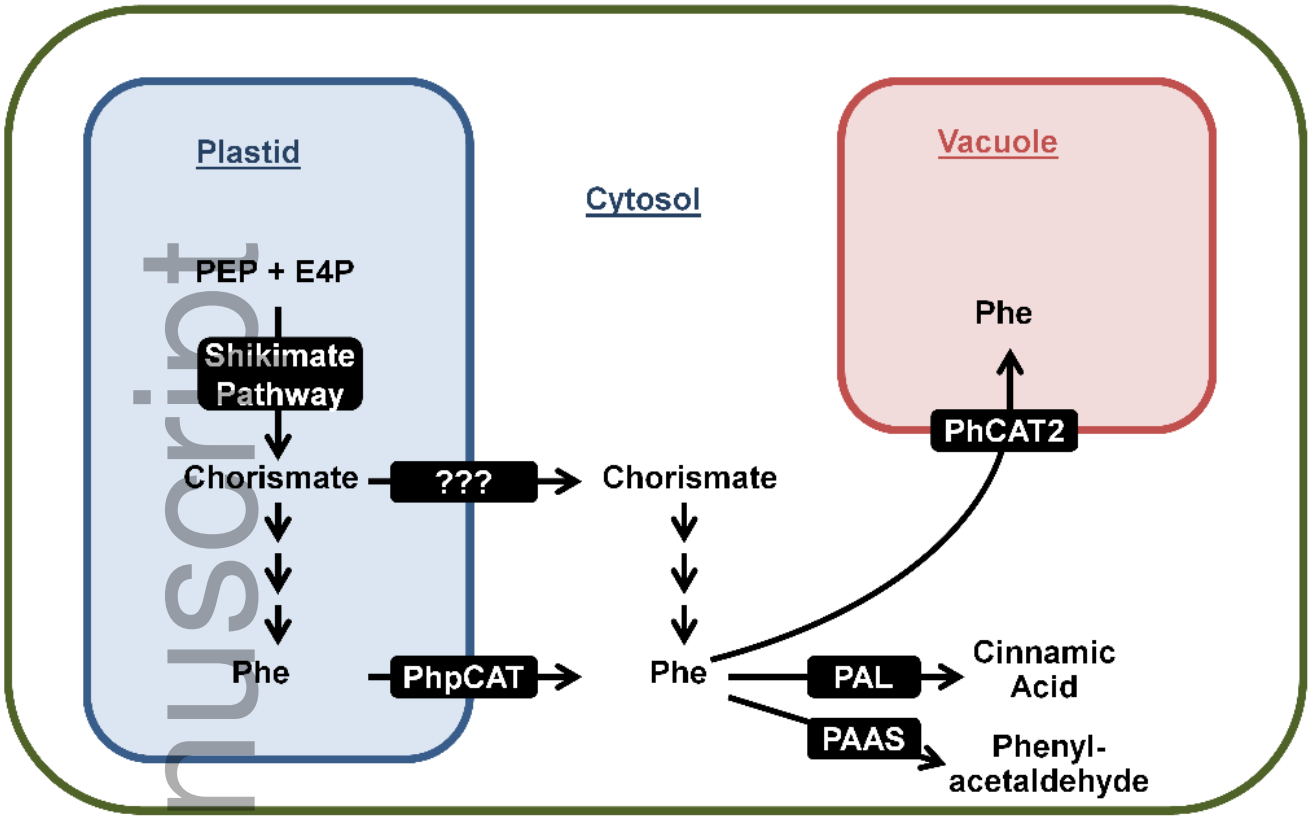

tpj_13730_f6.tif